Irradiated Recycled Plastic as a Concrete Additive for Improved Chemo-mechanical Properties in Hardened Cement Pastes

by

Carolyn Schaefer

SUBMITTED TO THE DEPARTMENT OF NUCLEAR SCIENCE AND ENGINEERING IN PARTIAL FULFILLMENT OF THE REQUIREMENTS FOR THE DEGREE OF

BACHELOR OF SCIENCE IN NUCLEAR SCIENCE AND ENGINEERING
AT THE
MASSACHUSETTS INSTITUTE OF TECHNOLOGY

JUNE 2017

Signature of Author:_____

Carolyn Schaefer
Department of Nuclear Science and Engineering
May 18, 2017

Certified by:_____

Michael Short
Assistant Professor of Nuclear Science and Engineering
Thesis Supervisor

and:_____

Oral Büyüköztürk
Professor of Civil and Environmental Engineering
Thesis Supervisor

Accepted by:_____

Michael Short
Assistant Professor of Nuclear Science and Engineering
Chairman, NSE Committee for Undergraduate Students

Irradiated Recycled Plastic as a Concrete Additive for Improved Chemo-mechanical Properties in Hardened Cement Pastes

by

Carolyn Schaefer

Submitted to the Department of Nuclear Science and Engineering on May 18, 2017
In Partial Fulfillment of the Requirements for the Degree of
Bachelor of Science in Nuclear Science and Engineering

Abstract

Portland cement based concrete production contributes heavily to greenhouse gas emissions. Thus a need exists for the development of durable and sustainable concrete with a lower carbon footprint. This can be achieved when Portland cement is partially replaced with another material without compromising the concrete's strength. The use of waste plastics in concrete has been explored as a means of improving concrete's mechanical properties while also providing an efficient way to both repurpose waste plastic and partially displace cement for the purpose of reducing carbon emissions. This replacement, however, typically comes with a sacrifice of compressive strength. This work discusses the design for and progress toward a high-strength concrete with a dense cementious matrix that contains an irradiated plastic additive. Cement samples containing various combinations of cement binder and plastic content were prepared; compressive strength tests showed that for all cement binder types, the addition of high dose irradiated plastic resulted in increased compressive strength as compared to the strengths achieved by samples with regular, non-irradiated plastic. This suggests that irradiating plastic at a high dose is a viable potential solution for gaining some of the strength back that is lost when plastic is added to concrete. To assess the internal structure of the samples and gain some insight into what aspects of their chemical compositions' contributed to the observed strength differences, a microstructural analysis—consisting of XRD, SEM, and X-ray microtomography—was performed. XRD analysis showed that various differences in C-S-H and C-A-S-H phase formation from the addition of both irradiated plastic and mineral additives helped to form high-density phases that contributed to higher relative strengths. BSE analysis showed that an increased alumina content among fly ash samples helped to form the high-density phases that contributed to higher relative strength among the fly ash samples, as evidenced through a ternary phase diagram. X-ray microtomography showed that the addition of high dose irradiated plastic consistently contributed to a decrease in segmented porosity, indicating that irradiated plastic may have acted as a pore-blocking agent. The results presented clearly show the benefit of using irradiated plastic as a concrete additive for improved compressive strength. By partially replacing Portland cement with a repurposed waste material, this design, when scaled to the level of mass concrete production, could contribute to reduced carbon emissions and provide a long-term solution for waste plastic storage.

Thesis Supervisors: (1) Michael Short, (2) Oral Büyüköztürk
Titles: (1) Assistant Professor of Nuclear Science and Engineering, (2) Professor of Civil and Environmental Engineering

Contents

List of Figures

Abbreviations

PET	Polyethylene terephthalate
C-S-H	Calcium silicate hydrate
OPC	Ordinary Portland Cement
FA	Fly ash
SF	Silica fume
Ctrl	Control
RP	Regular plastic
LD	Low dose
HD	High dose
XRF	X-ray fluorescence
PSD	Particle size distribution
XRD	X-ray diffraction
SEM	Scanning electron microscopy
BSE	Back scattered electron
EDS	Energy dispersive spectroscopy
C-A-S-H	Calcium aluminum silicate hydrate
ASR	Alkali silica reaction
VOI	Volume of interest

1 Introduction

The use of recycled plastics in concrete has been explored as a means of improving concrete's mechanical properties while also providing an efficient way to both repurpose waste plastic and partially displace cement for the purpose of reducing carbon emissions. The task remains, however, to develop a cement design that allows for both the addition of plastic and the preservation of high compressive strength. This study explores the effectiveness of gamma-irradiated plastic as an additive in cement paste samples for improving compressive strength. Irradiated plastic is paired with different mineral additives, which are commonly used to achieve high strength, with the goal of finding an optimal combination. An internal microstructural analysis is presented in order to provide some insight into the aspects of the materials' chemical compositions that contribute to the observed variation in strength. The objective is to determine whether or not irradiated plastic is an effective partial replacement for cement; achieving a high-strength concrete using this additive would imply the ability to produce a lower carbon footprint concrete variety that could even act as a permanent storage option for plastic waste.

2 Background

2.1 Carbon Emissions in the Cement Industry

Concrete is the second most widely used material on the planet, after water [1]. The cement industry accounts for roughly 5% of global anthropogenic carbon dioxide emissions, making it a critical sector for emissions mitigation [2]. The production of Portland cement releases carbon dioxide both directly and indirectly. Direct emissions result from a process known as calcination, which occurs when limestone, the primary component of cement, is heated [3]. The calcium carbonate in the limestone breaks down into calcium oxide and carbon dioxide. This process accounts for roughly half of all emissions from cement production. To produce cement, limestone and other clay-like materials are heated in a kiln at around 1400°C. Indirect emissions result from the burning of fossil fuels to heat the kiln and account for about 40% of cement production emissions. The electricity used to power additional plant machinery, as well as the final transportation of cement, account for the remaining 10% of total emissions. These emissions make partial replacement of cement with a substitute material an attractive alternative to alleviate the negative environmental impact of cement production.

2.2 Plastic Waste and Recycling

Constituting a separate environmental issue is the abundance of plastic waste. Plastics have come to play an essential role in our everyday lives. Their favorable properties, including low cost, high strength-to-weight ratio, and low density make them ideal for use in a wide range of products [4]. It has been shown that over half of global plastic production is used for one-off disposable consumer products. This contributes heavily to the production of plastic-related waste, most of which is not biodegradable and will not react chemically in natural settings, and therefore it remains in the environment for decades or even centuries. Plastic wastes have become universally accepted as a serious environmental issue.

Despite improvements in technology and awareness that have occurred since the recycling of plastic waste began in 1980, the recycling rate of post-consumed plastic wastes is still fairly low [5]. A 2012 study showed a plastic recycling rate of only 8.8%, while the remaining 91.2% was simply discarded. The discarded plastic is typically put into a landfill, which is considered the least desirable method of dealing with plastic waste because it demands heavy space consumption and contributes to long-term pollution [4]. In some countries waste plastic is incinerated for energy recovery because of its high calorific value. This method, however, produces toxic ash and releases carbon dioxide and poisonous chemicals into the environment. Recycling, therefore, is seen as the ideal solution for minimizing environmental impact. Among the various approaches to managing recycling are (1) standard mechanical recycling, which aims to recover plastic via mechanical processes (sorting, grinding, cleaning, drying, re-granulating, etc.) and produces recyclates that can be transformed into new plastic products, and (2) recycling in the form of repurposing the waste plastic without fully breaking it down [6]. Mechanical recycling degrades the quality of the plastic during the service cycle, and often times the plastic that is recycled in the United States is exported, with about two-thirds being shipped to China [4,7]. This is due to the fact that the U.S. recycling market is small in comparison to other countries [8]. The exported plastic is shipped overseas via massive cargo ships, which collectively release billions of tons of CO_2 annually, along with considerable amounts of nitrogen and sulfur [9]. Thus reusing waste plastic in other industries is considered a more ideal method of disposal [4].

2.3 Plastic as an Additive in Concrete

Recently, researchers have explored waste plastic's potential as an environmentally friendly construction material by repurposing it as an additive in concrete mix and studying the concrete's resultant behavior [4]. Specifically, polyethylene terephthalate (PET) has been explored as a lightweight concrete aggregate that could improve various mechanical properties and replace the standard lightweight aggregates that are typically

used, which face some problems related to both cost and quality [10]. PET is a polymer notable for being the constituent of the clear plastic used for soda and water bottle containers. It has been shown that the use of PET in concrete can improve the concrete's flexural toughness, impact resistance, and workability [10,11]. Various studies have shown mixed results for improvements in tensile strength [11, 12]. Compressive strength, however, has generally been shown to decrease with the addition of PET. Thus it is apparent that the task remains to produce a PET-enhanced concrete capable of demonstrating the aforementioned mechanical improvements without compromising its compressive strength.

2.4 Gamma Irradiation of PET

One potential solution for gaining some of the strength back that is lost when plastic is added to concrete is to make use of irradiation to improve the plastic's strength properties. PET is a semi-crystalline polyester that exhibits an isotropic microstructure due to its glassy amorphous composition [13]. For this reason, it is one of the most studied polymers. Upon irradiation, the two effects of greatest importance for PET are chain scission and crosslinking [14]. It has been shown that, due to the chain scission effect, the degree of crystallinity in PET increases with gamma radiation dose [15]. The number of chain scissions increases with dose, thereby decreasing the molecular weight. This reduced weight accounts for improved molecular mobility, which facilitates the ordered arrangement of molecules in crystalline structures. Thus the increase in mobility as a result of chain scission leads to greater crystallizability when PET is irradiated by gamma rays. The extent of crystallinity has a significant impact on several mechanical properties of PET [16]. Higher crystallinity PET has been shown to have higher modulus, toughness, stiffness, strength, and hardness. Alternatively, crosslinking is the chemical bonding of one polymer chain to another [14]. It can be induced by radiation and has the effect of strengthening the chemical structure of the compound. Thus both chain scission and crosslinking (which can occur simultaneously) in PET can result in its improved strength.

2.5 Industrial Byproducts as Current High Strength Options

Industrial byproducts such as silica fume, a byproduct of the silicon production, and fly ash, a byproduct of coal combustion are commonly used to enhance concrete strength and water permeability characteristics [17]. This is useful both for creating High Performance Concrete and for minimizing the potential hazardous effects these byproducts have on the environment. These additives, when used in a concrete admixture, combine with calcium hydroxide liberated during cement hydration to form additional calcium silicate hydrate (C-S-H), the glue that strengthens and holds concrete together [18]. This additional C-S-

H densifies the cementitious matrix, thereby enhancing strength. When used to partially replace Ordinary Portland Cement (OPC) in cement mixtures, these supplementary cementitious materials act to decrease water penetration and improve concrete's compressive and tensile strength considerably, thus creating a feasible alternative for fabricating sustainable and durable cementitious materials.

2.6 Research Objective and Justification of This Study

A cement design that allows for both the addition of plastic and the preservation of high compressive strength remains to be discovered. This research aims to examine the effectiveness of irradiated plastic as an additive for enhancing the mechanical properties of concrete. Because gamma irradiation of PET is known to result in a strengthened chemical structure, there is reason to believe that an irradiated plastic additive would take advantage of the improvements in concrete's mechanical properties due to plastic alone as well as the polymer strength improvements resulting from irradiation. The collective effects are likely to provide a better solution than either contribution might achieve on its own. Within this scope is an additional objective of understanding the effect of the plastic's radiation dose on concrete strength by examining the effect of dosage on the cementious matrix itself. Furthermore, because the addition of an industrial byproduct is necessary to achieve high strength concrete, this work seeks to optimize the combination of both additive types—plastic and either fly ash or silica fume—by testing a series of dose-byproduct pairings for improved compressive strength. Phase identification through X-ray diffraction analysis, imaging through scanning electron microscopy, and pore structure analysis via 3D imaging through X-ray micro computed tomography are utilized to collectively assess the internal structure of the samples and to help determine which aspects of the materials' compositions contribute to variability in strength and porosity. This multiscale approach is used to characterize the complex matrix developed within the cement due to the addition of both additive types.

As discussed in Section 2.1, the manufacture of Portland cement is an energy intensive process that releases large amounts of carbon dioxide into the atmosphere. In the design presented here, the sample compositions are such that the plastic additive displaces a fraction of OPC. Because OPC production contributes so heavily to carbon emissions, achieving a high-strength concrete using an irradiated plastic additive would provide a solution that not only takes advantage of the known mechanical improvements resulting from the addition of plastic but also serves as a lower carbon footprint concrete variety that could even act as a permanent storage option for plastic waste.

3 Materials and Methods

A series of cement paste samples were prepared, each with a different combination of mineral additive and plastic type. After a 28-day cure period, these specimens underwent compression testing to determine the variation in their strengths. To assess the internal structure of the samples and gain some insight into what aspects of their compositions' contributed to the observed strength differences, a microstructural analysis—consisting of XRD, SEM, and X-ray microtomography—was performed.

3.1 Cement Samples Mix Design

The complete mix design for the concrete samples is shown in Table 1. Included are three different cement binders: Ordinary Portland Cement (OPC), OPC with Class F fly ash (OPC+FA), and OPC with silica fume (OPC+SF). For each binder, there were low-dose, high-dose, and no-dose combinations. Each individual combination was triplicated so that an average compressive strength with an uncertainty could ultimately be determined. For each of the non-control samples, the plastic made up 1.25% of the dry mass (see Appendix A for justification of this percent composition). For samples containing both the plastic additive and one of the mineral additives as the binder, the plastic only displaced the cement dry mass; the mineral additive consistently made up 15% of the total dry mass. According to previous studies, compressive strength of both silica fume and fly ash is maximized when these additives provide around 15% of the mass [19, 20].

Table 1. Mix design of the cement paste samples

Binder	Type	Total Dry Mass (g)	Plastic (g)	OPC (g)	Class F (g)	Silica Fume (g)
OPC	Ctrl	1400	0	1400	0	0
OPC	RP	1400	17.5	1382.5	0	0
OPC	HD	1400	17.5	1382.5	0	0
OPC	LD	1400	17.5	1382.5	0	0
OPC + FA	Ctrl	1400	0	1190	210	0
OPC + FA	RP	1400	17.5	1172.5	210	0
OPC + FA	HD	1400	17.5	1172.5	210	0
OPC + FA	LD	1400	17.5	1172.5	210	0
OPC + SF	Ctrl	1400	0	1190	0	210
OPC + SF	RP	1400	17.5	1172.5	0	210
OPC + SF	HD	1400	17.5	1172.5	0	210
OPC + SF	LD	1400	17.5	1172.5	0	210

FA = Fly ash, SF = Silica fume, Ctrl = No plastic, RP = Regular plastic, HD = High dose plastic, LD = Low dose plastic

3.2 X-Ray Fluorescence (XRF) Spectroscopy and Particle Size Distribution (PSD) Analysis

An analysis of the chemical breakdown and the particle size for both OPC and the two mineral additives was desired for the purpose of obtaining a complete record of the materials used in this study. The chemical compositions of OPC, Class F fly ash, and silica fume were measured using X-ray Florescence (XRF) spectroscopy. The results are shown in Table 2. The sum of the silicon oxide (SiO_2), aluminum oxide (Al_2O_3), and ferric oxide (Fe_2O_3) components of the fly ash is 90.01%, indicating that this material is a Class F type of ash according to ASTM C 618 [21]. Particle size distribution (PSD) was conducted on all three materials by suspending them in isopropyl alcohol using a Laser Light Scattering technique with a particle size analyzer. The mean particle sizes for OPC, Class F fly ash, and silica fume were found to be 12.73, 38.50, and 12.05 μm, respectively.

Table 2. XRF composition and particle size of the Portland cement, Class F fly ash and silica fume

Chemical Composition (%)	CaO	SiO_2	Al_2O_3	MgO	SO_3	TiO_2	K_2O	Fe_2O_3	Na_2O	MnO	SrO	Mean Particle Size (μm)
Binder Type												
OPC	62.27	16.63	3.63	1.22	3.91	0.24	0.61	3.28	0.34	0.06	0.07	12.73
Class F FA	3.82	61.72	19.07	1.57	0.25	2.44	1.27	9.22	0.68	-	-	38.50
SF	1.2	85.50	1.61	1.4	0.40	<0.05	0.65	1.89	0.43	0.01	0.01	12.05

SF = Silica Fume, FA = Fly Ash, OPC = Ordinary Portland cement (OPC)

3.3 Preparation of Irradiated Plastic Additive

For considerations of dose level in the context of this design, previous studies were used to determine the effect of gamma irradiation on the strength properties of plastic at varying doses. Literature review showed that different types of strength were maximized in different dose ranges [22, 14, 23, 24]. These dose-strength relationships are summarized in Appendix B. Specifically, one study showed that tensile strength increased up to 10 kGy [14], while another reported that radiation-induced crosslinking improved strength for doses up to 150 kGy [22]. Consequently, it was decided that a high dose of 100 kGy and a low dose of 10 kGy should be tested and compared. These levels determine the length of irradiation time for the desired high- and low-dose plastic additives.

Plastic flakes obtained from a recycling facility were used for the plastic additive. Due to imperfections in recycling facilities' sorting processes, the sample originally contained pieces of metal and other non-plastic impurities. In an effort to eliminate the possibility that these impurities would contaminate or ruin the future cement samples, the plastic was manually sorted to remove all materials that were clearly not plastic. Half of the plastic was then irradiated in a cobalt-60 irradiator facility that operates at 58 Gy/min. The low dose sample was left in the machine for 2.9 hours for a total of 10 kGy. The high dose sample was left in the machine for 28.7 hours for a total dose of 100 kGy. The flakes were then further crushed using both a high-energy ball mill and a mortar and pestle. Previous studies have shown that the compressive strength of PET-enhanced cement decreases with PET particle size (for samples with a 28-day cure) [25]. The objective for the crushing process was therefore to achieve a particle size that was as small as possible. Each 18-gram sample was processed for 2 hours in the ball mill followed by 20 minutes with the mortar and pestle. The actual particle size at the end of the process was not uniform, and an average particle size of 170 microns was measured using an optical microscope.

The effect of the irradiation process on the PET's amorphous content was determined by calculating the amorphous and crystalline contributions for each of the three plastic types: high dose, low dose, and no dose. Powder X-ray diffraction (XRD) provides a means of determining the relative amorphous content for most materials. XRD was performed on all three plastics (see Section 3.6 for XRD preset specifications and experimental setup, which were the same for the plastics and the cement samples). To quantify the amorphous contribution, High Score Plus software from Pan Analytical was used to analyze the diffraction patterns. The quantification technique used was taken from Klug and Alexander, 1974 [26]. This method is illustrated in Figure 1. Though this quantification method does not necessarily produce absolute results, it allows for a batch-to-batch comparison for observing trends in the amorphous content. As shown, the crystalline portion appears to increase with dose, with the high-dose plastic showing roughly 48% crystallinity[1]. This trend in dose-crystallinity relationship was consistent with expectation (see Section 2.4). The increased crystallinity may have contributed to the higher strengths that were observed in the specimens containing irradiated plastic (see Section 4.1).

3.4 Preparation of Cement Paste Samples

Cement paste samples were constructed using a basic process in which the components were mixed with a kitchen mixer and poured into 2 in. by 4 in. cylindrical molds, a standard for compressive strength testing. After 24 hours, the samples were removed from the molds and placed in tubs of water where they cured for 28 days. Curing is necessary to maintain moisture levels inside cement so that hydration can continue. After 28 days, very little unhydrated cement exists, so most of the possible strength is attained at that time [27]. Once fully cured, the samples were submerged in acetone for 48 hours in order to halt the hydration process.

[1] A Rietveld analysis was originally planned for quantification of the amorphous content. Thus the plastic samples also contained 10% by weight of corundum powder. The nature of the diffraction patterns made them more suited for the graphical approach used, but it should be noted that the values obtained for the amorphous and crystalline contents in all three plastic are due in part to the 10% by weight inclusion of the corundum.

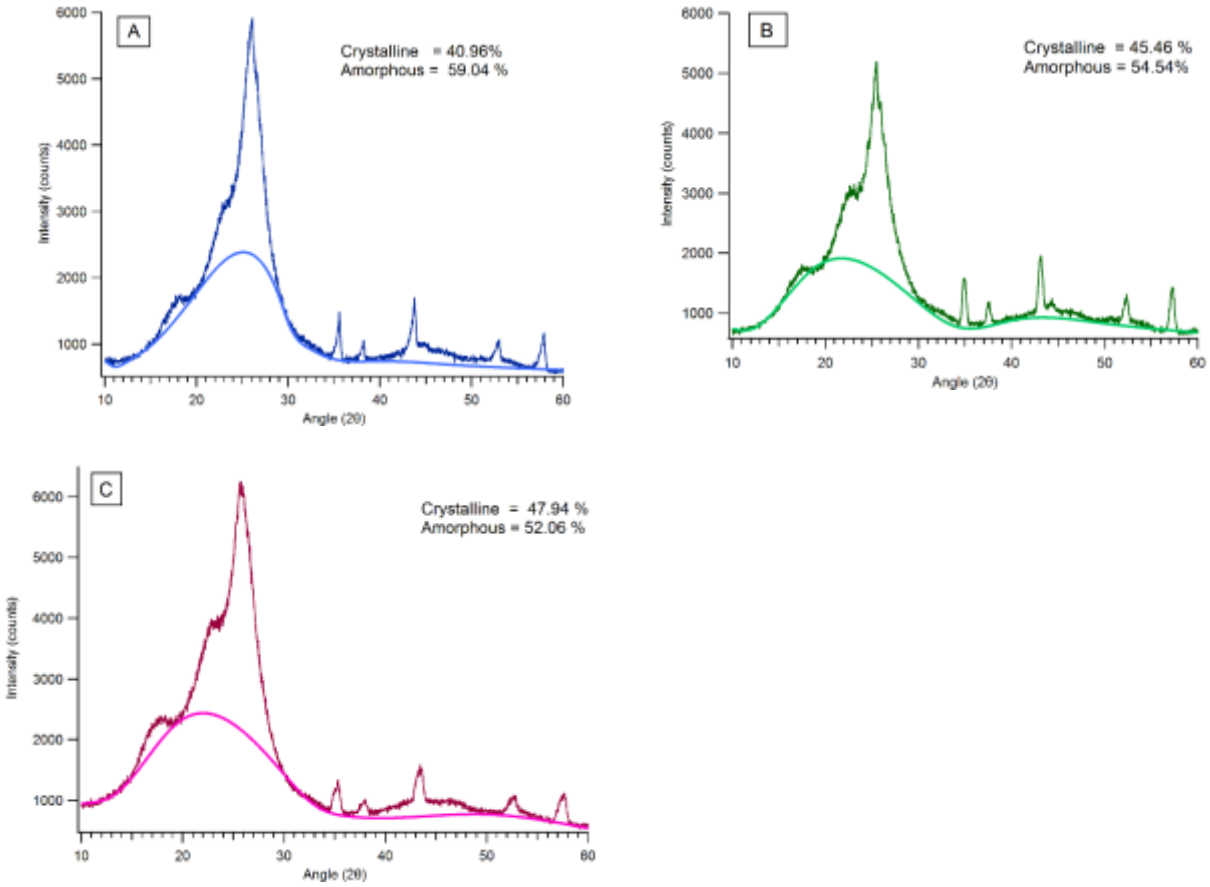

Figure 1. Crystalline and amorphous values obtained for (a) regular plastic, (b) plastic exposed to low dose and (c) plastic exposed to high dose. In the technique applied, the user discriminates between the gradual baseline changes due to the amorphous content (shown by the lighter colored lines) and the background scatter so that the portion above the baseline that separates the crystalline from the amorphous components can be subtracted out, and the diffraction intensity for the amorphous content alone can be determined [26].

3.5 Compression Testing

Compressive strength testing is a common performance measure for concrete; it provides immediate information on the bulk strength of the specimen being tested. It is also an essential step for gaining critical insight into the potential qualitative relationship between the desirable characteristics of concrete and its strength. Compressive strength is measured by breaking cylindrical concrete specimens in a compression test machine to determine the maximum pressure load the specimen can withstand.

To provide an evenly distributed load on the cement specimens, plaster was applied to both ends of each cylinder and allowed to set for 24 hours. The testing setup is shown in Figure 2. The specimens were subjected to a compression test as per ASTM C 39 [28]. A 0.20 MPa/sec loading rate was selected and kept consistent throughout the testing procedure. (ASTM C 39 regulates 0.15-0.25 MPa/sec as the standard rate for

cylindrical specimens.) The maximum normal stress before failure was measured and recorded. This stress measurement is equivalent to the compressive strength of the sample. This procedure was performed for each of the three samples of the twelve cement-plastic combinations.

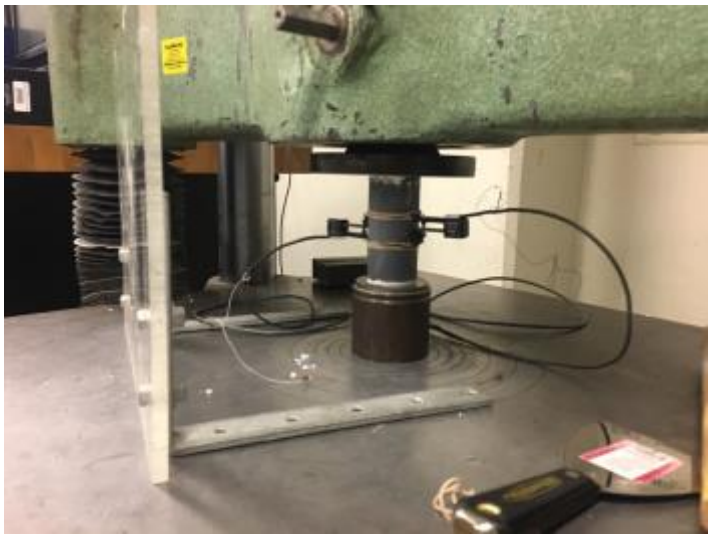

Figure 2. Compressive strength testing setup. The cylindrical sample was compressed until fracture, at which point the maximum normal stress was recorded in units of pressure. 36 samples in total were tested.

3.6 X-Ray Diffraction (XRD)

The specimens, fractured from compression testing, were crushed into a powder so that XRD could be performed for the purpose of identifying and quantifying crystalline phases that might be contributing to the observed variation in strength. The highest strength sample of the three for each of the twelve additive combinations was used for this portion of the study (and for all remaining portions). XRD was conducted with an X-ray diffractometer that uses a Cu K-alpha radiation nickel foil filter. The ground sample was placed on Bragg–Brentano geometry optics on a flat plate sample geometry. A fixed divergence slit of 1/16 degree was chosen to limit beam overflow on the samples at small angles of 2h. Incident and diffracted-side soller slits of 0.02 rad were used for this experiment. The X'Celerator high-speed linear detector was used with an active length of 2.122 degrees 2h, a step size of 0.0167113 degrees 2h, and a scan range from 4 to 90 degrees. High Score Plus software from Pan Analytical was used to carry out the semi-quantitative studies using Rietveld analysis [29].

3.7 Back Scattered Electron (BSE) and Energy Dispersive Spectroscopy (EDS) Analysis

Back Scattered Electron (BSE) imaging was performed on polished samples to examine the additives' effect on the structure and chemistry of the cementitious matrix. For polishing, small fragments from the cement paste samples were epoxy impregnated and polished to 50 nm surface roughness. In BSE, beam electrons are reflected from the sample via elastic scattering. The images created can provide essential information about the distribution of various elements within the sample. A field-emission scanning electron microscope (FE-SEM) by ZEISS was used to carry out the BSE analysis. EDS elemental- and phase-mapping were also carried out on these samples. EDS is a technique used for the chemical characterization that derives its analytical capabilities from measurement of the photon energy emitted from the specimen. Because each element has a unique atomic structure, and therefore a unique electromagnetic emission spectrum, it is possible to characterize individual elements and phases through EDS. Elemental- and phase-maps for each of the twelve polished samples were acquired using this technique.

3.8 X-Ray Microtomography (X-Ray μCT)

Fragments of the hardened cement paste samples were prepared as approximately 1 mm length cubes and examined using X-ray microtomography at Beamline 2-BM at the Advanced Photon Source, Argonne National Laboratory. X-ray microtomography allows for a full three-dimensional visualization of the samples by combining a series of two-dimensional images. The experimental setup is shown in Figure 3. Measurements were carried out with a parallel beam configuration using a hard X-ray synchrotron radiation of 25 keV. The samples were mounted between polymeric cones to permit alignment, and all the samples were within the field of view in the horizonatal plane of the detector, as shown in Figure 3. X-ray detection was obtained with a scintillator and a charge coupled device (CCD) camera with a resolution of 1920 × 1200 pixels and a voxel resolution of 5.86 μm. It was coupled to two different ZEISS lenses (x2.5 and x5 magnification), resulting in scans of 2.09 and 1.08 μm of pixel size, and it consisted of 4,501 projections obtained through 180 degrees rotation, with a variable exposure time of 0.2 to 0.4, depending on the size of the sample.

A major advantage of X-ray microtomography lies in the ability to extract the three-dimensional morphology of the pore network, which allows for the determination of segmented and effective porosity for the samples. Segmented porosity is associated with the extracted pore space without any consideration of connectivity, whereas effective porosity is the sum total of the interconnected pore space. As an example, Figure 4 shows a two-dimensional slice of the complete tomographic reconstruction of a representative sample, which was prepared with the OPC+FA-Ctrl sample. Additional image analysis and segmentation using IMAGEJ 1.48 software were performed in order to calculate the porosity, as detailed in Section 4.4.

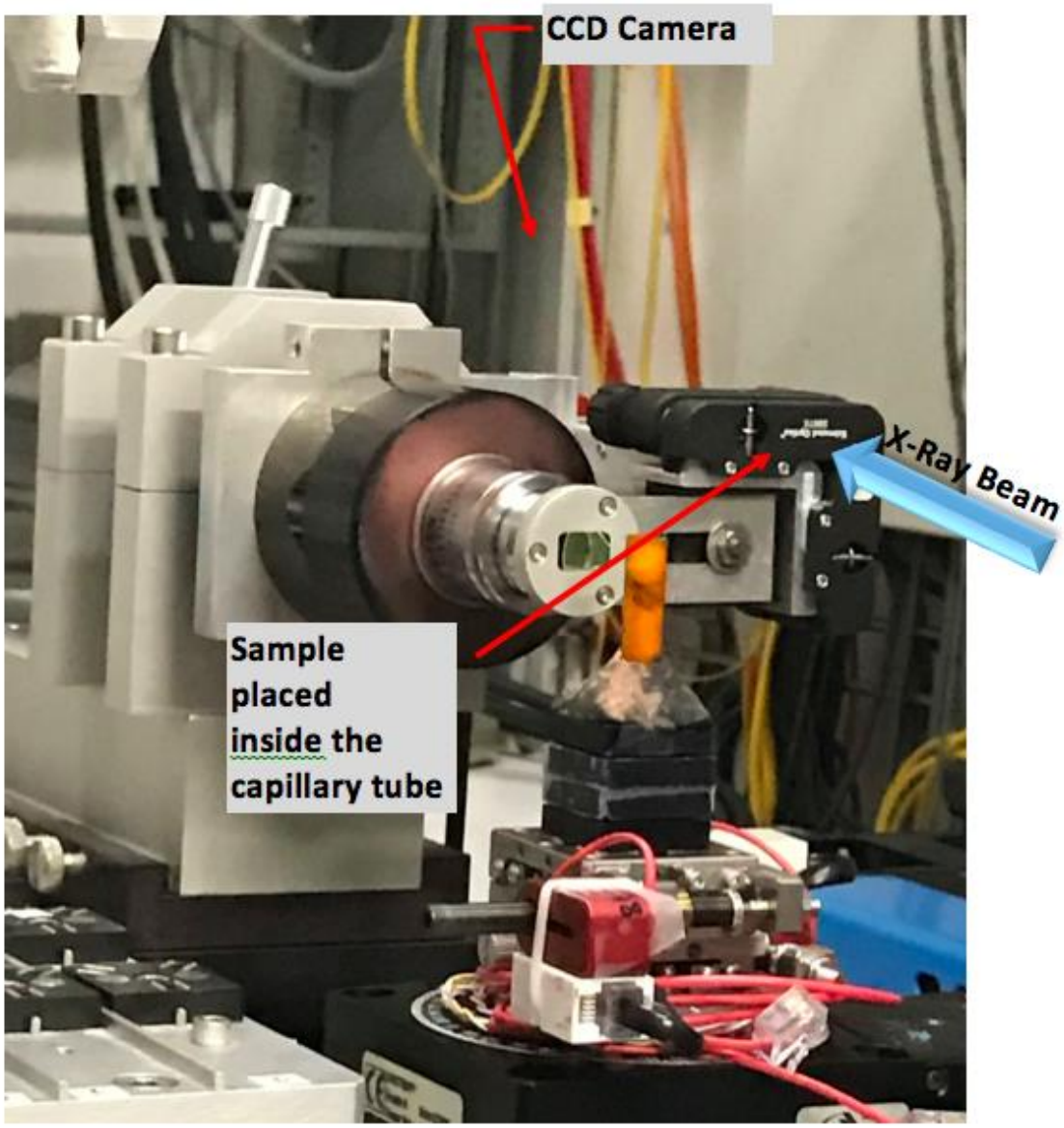

Figure 3. Experimental set-up used at Beamline 2-BM at the Advanced Photon Source at Argonne National Laboratory, Illinois. The samples were fragments of the hardened cement past samples, which had been prepared as ~1 mm length cubes.

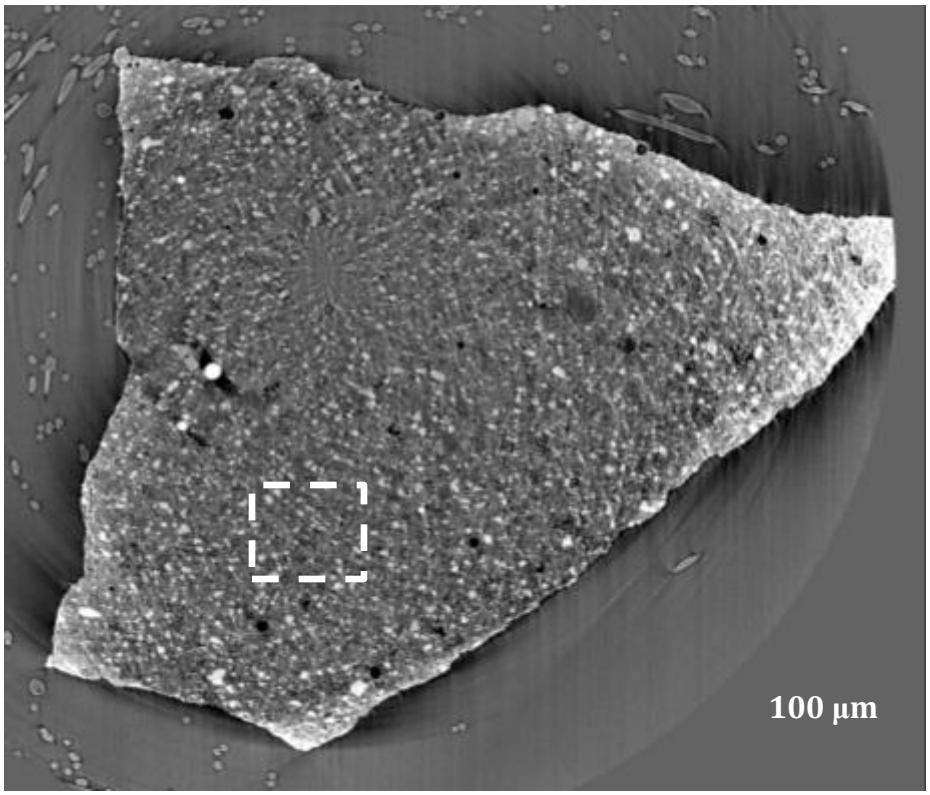

Figure 4. A slice through the complete tomographic reconstruction of the OPC+FA-Ctrl sample

4 Results and Discussion

4.1 Compression Test Analysis

The results of compression testing for all samples are shown in Figure 5. Through comparison of the first three bars, which represent the controls, it is clear that the inclusions of fly ash and silica fume alone contributed to increases in strength of 36% and 14%, respectively, as compared to the OPC control. As expected, for all three binder types the inclusion of regular plastic resulted in strengths significantly lower than those of the plastic-free controls. It is interesting to note that inclusion of high dose irradiated plastic in all three binder types (OPC-HD, OPC+FA-HD, OPC+SF-HD) resulted in increased compressive strength as compared to the samples containing non-irradiated plastic (OPC-RP, OPC+FA-RP, OPC+SF-RP). This effect was most drastic for OPC samples, for which the addition of high dose irradiated plastic (OPC-HD) contributed to an increase in strength of 20% as compared to OPC-RP. This consistent increase can be attributed in part to the increase in crystallinity of the PET due to irradiation, as shown in Figure 1.

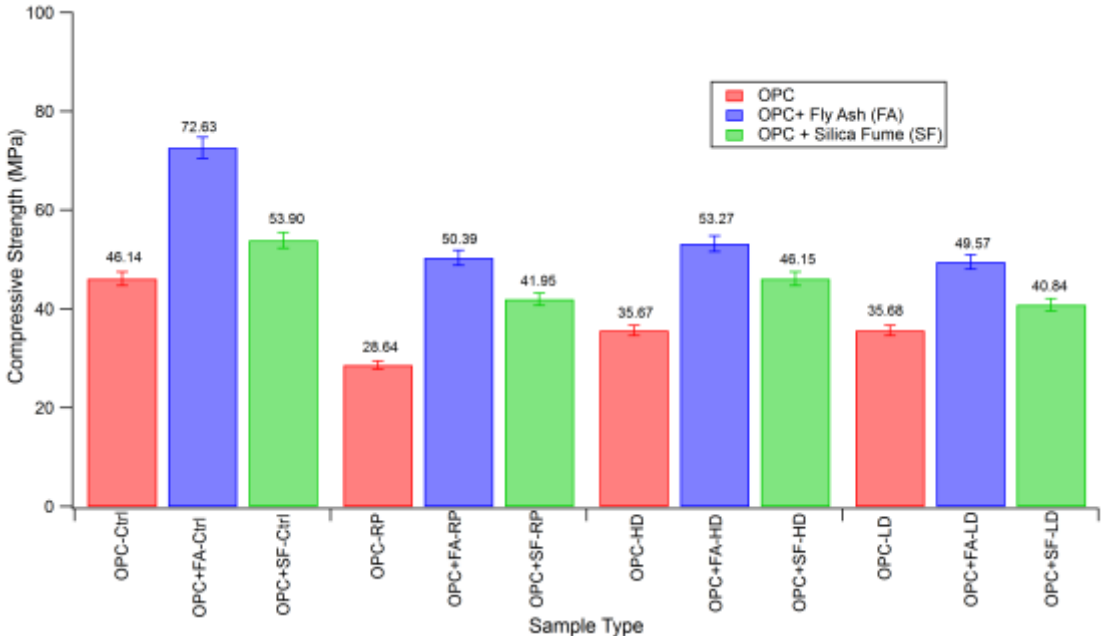

Figure 5. Compressive strength analysis for all specimens. The bars represent the averages of the three samples for each combination. An increase of strength from regular plastic to high dose irradiated plastic is observed for all three cement binder types.

The effect of the mineral additives alone on compressive strength was also demonstrated, as the inclusion of fly ash led to the highest strengths for all four plastic conditions (Ctrl, RP, LD, HD), followed by silica fume samples. The OPC samples showed the lowest strength for all four plastic conditions. Thus the additional calcium silicate hydrate (C-S-H) formation, which contributes to strength increases, is likely due to the inclusion of both additive types: the mineral additives and the irradiated plastic. The results presented in further sections detail this phase formation using XRD and EDS (via BSE) analysis; they serve to provide a microstructural insight into this variation in compressive strength.

4.2 X-Ray Diffraction Analysis

The XRD spectra for the four OPC samples (Ctrl, RP, LD, HD) are shown in Figure 6. As is commonly observed in hydrated OPC, calcium silicate hydrate (C-S-H) phases, including rosenhahnite, were detected. In addition, Portlandite, a crystalline form of calcium hydroxide, along with calcite was observed among the samples. The sulfate related phases that were present were thenardite and calcium sulfate hydrate (also known as gypsum). Dolomite and quartz were also observed. It is interesting to note that the addition of low dose irradiated plastic led to a change in the crystal structure of C-S-H by

forming the gismondine phase, which is related to calcium aluminum silicate hydrate (C-A-S-H) gels. This was not observed in the OPC-Ctrl or OPC-RP samples, suggesting that the addition of irradiated plastic caused a change in the structure of C-S-H gels and initiated the possible formation of unique aluminum-incorporated C-S-H gels.

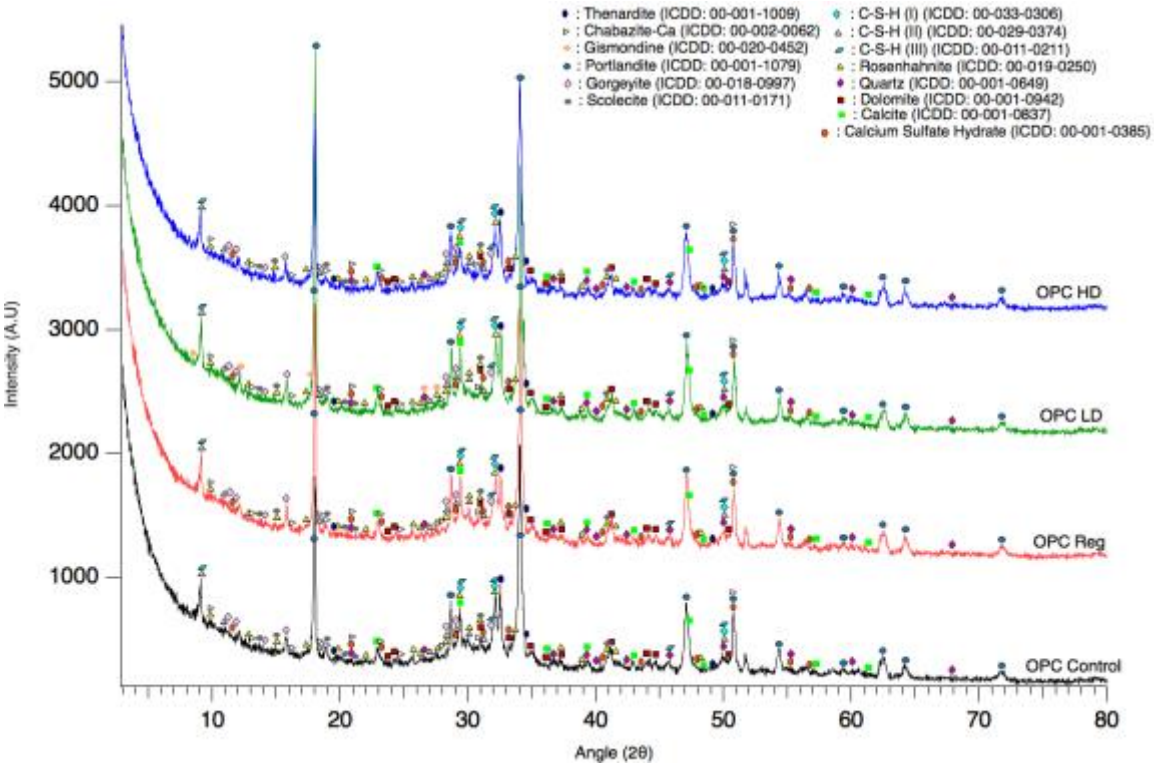

Figure 6. XRD analysis for OPC samples prepared with regular, low dose, and high dose plastic. The gismondine phase was only present in the low dose sample.

The XRD spectra for the four OPC+FA samples (Ctrl, RP, LD, HD) are shown in Figure 7. Many of the same phases as in OPC were apparent. The okenite phase, which is related to a zeolite type mineral, was only present in the OPC+FA-Ctrl sample. Okenite, an uncommon reaction product, has also been observed as one of the crystallization products for alkali silica reaction (ASR) gels [30]. However, it cannot be confirmed given the phases apparent here that the presence of okenite led to any ASR gel formation. Furthermore, the addition of irradiated plastic allowed for different forms of C-A-S-H gel formation (gismondine and chabazite-Ca were present), though in this case those phases were detected in the OPC+FA-Ctrl and OPC+FA-RP samples, as well.

The XRD spectra for the four OPC+SF samples (Ctrl, RP, LD, HD) are shown in Figure 8. Again, many of the same phases as in OPC and OPC+FA were apparent. The presence of gismondine was detected only in the OPC+SF-LD and OPC+SF-HD samples. Thus irradiated plastic along with the addition of silica fume could have contributed to unique C-A-S-H gel formation. The gismondine phase, specifically, is attributed the storage of chemically bound water incorporating ions of calcium and

silicon in small cages, which can later contribute to additional hydration and an increase in strength of the cement matrix [31]. It is possible, then, that this effect explains the strength increase observed for the OPC+SF-HD sample as compared to the OPC+SF-RP sample.

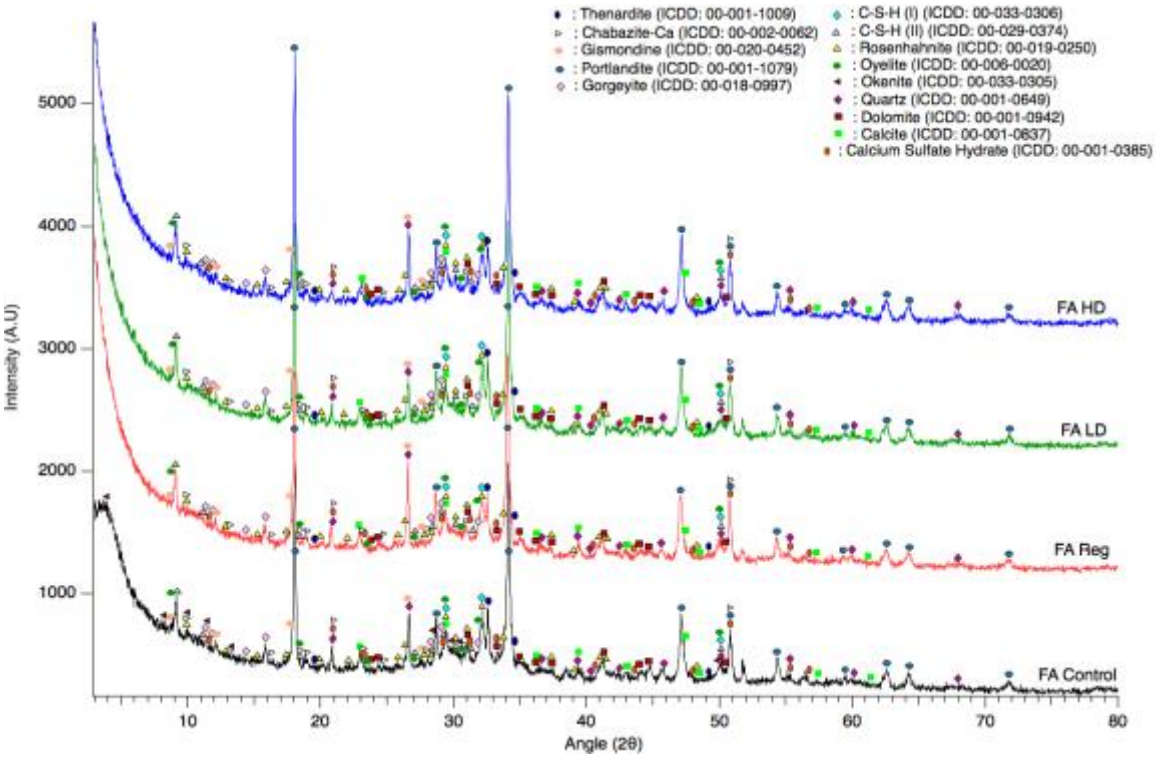

Figure 7. XRD analysis for OPC + FA samples prepared with regular, low dose, and high dose plastic. The okenite phase was only present in the control sample.

In addition to differences within each binder type due to the various plastic additives, there were also distinct dissimilarities apparent in the comparison between OPC, OPC+FA, and OPC+SF. C-S-H type III was present only among the OPC samples, whereas oyelite was observed only in OPC+FA samples. Studies have shown that the presence of oyelite commonly occurs along with 11 Å tobermorite, and its occurrence could have been due to the addition of fly ash. There is also a known association of plombièrite and oyelite in the deposit, because of which an amount of B_2O_3 has been reported in some analyses of plombièrite [32]. It is unclear, however, whether or not this occurred within the OPC+FA samples or if such an effect could have contributed to the observed strength increases resulting from the addition of fly ash.

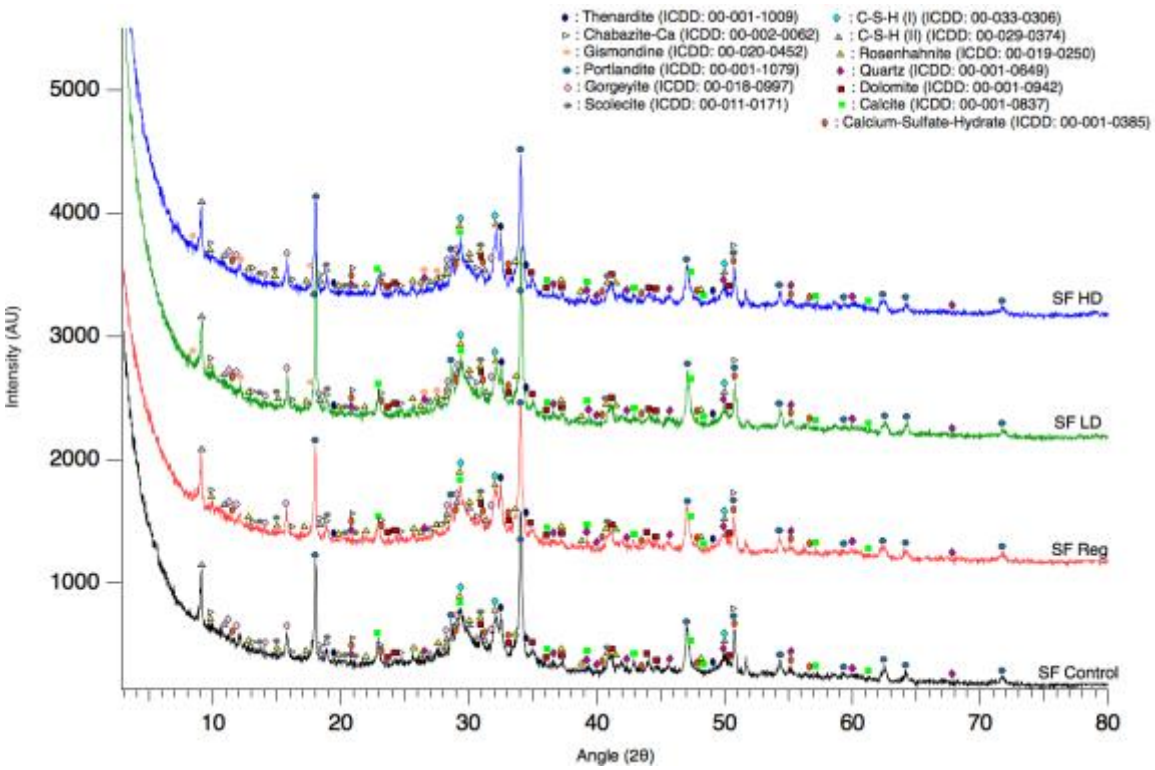

Figure 8. XRD analysis for OPC + SF samples prepared with regular, low dose, and high dose plastic. The gismondine phase was only present in the low dose and high dose samples.

4.3 Backscattered Electron (BSE) and Ternary Phase Diagram Analysis

BSE analysis on hardened polished samples for OPC+FA combinations is shown in Figure 9. The advantage of BSE is the ability to achieve a wide range of magnifications in order to examine the individual hydration products [33, 34]. During the cement hydration process, the free water reacts with the clinker forming chemically bound water, which is formed in C-S-H gels. It can be seen in Figure 9 that there is a water-filled space of outer product of C-S-H and calcium hydroxide crystals, along with alite (C_3S). A central grain of belite (C_2S) that is ~4 μm in size is also visible. It shows the classic striations that arise from crystal twinning and that are highly temperature dependent [34]. It is also important to note that the Portland cement powder contains pure C_3S (tricalcium silicate, or alite), C_2S (dicalcium silicate, or belite), C_3A (tricalicum aluminate), and C_4AF (tetracalcium aluminoferrite), but hydration forms these into impure forms. Thus the alites and belites pointed out in Figure 9, which are products formed during hydration, are impure forms of these compounds.

Inclusion of fly ash led to spherical morphology of unreacted fly ash that may not have been involved in the hydration process. Figure 9c shows that fly ash grains appear to be hollow, and it is possible that hydrates have filled inside the grains. Dark rims of magnesium containing hydrotalcite-like phases were also observed in these samples. The darker grey areas in the BSE image are made up of enriched carbon and oxygen, and they are assigned to carbonates.

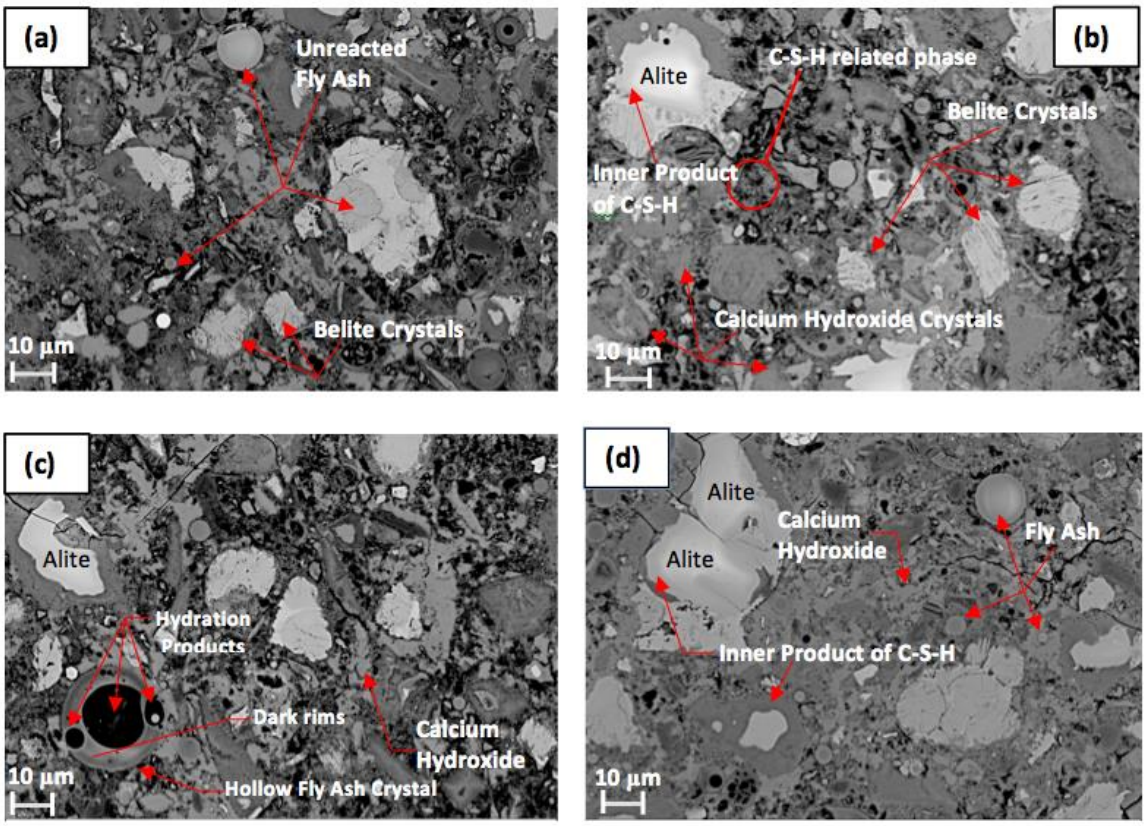

Figure 9. BSE analysis on hardened polished samples of (a) OPC+FA-Ctrl, (b) OPC+FA-RP, (c) OPC+FA-LD, and (d) OPC+FA-HD

EDS analysis was used to perform elemental and phase analysis for all samples. As an example, the results for the OPC+FA-LD sample are shown in Figure 10. The elemental analysis helps determine the distribution certain elements of interest, including oxygen, aluminum, calcium, and silicon, as shown in Figure 10b. A fairly a new techniques developed within EDS shows a phase map which detects the phases and semi-quantitatively calculates the percentage of phase present in the hydrated sample. This analysis, depicted in Figure 10c, can provide additional verification of the XRD studies that were reported in the section 4.2.

Figures 9 and 10 are included for visualization purposes; observation of BSE images and comparison of elemental- and phase-mapping among the different specimens can provide only a qualitative insight. A more definite comparison can be made visually

with a ternary phase diagram, the use of which is a powerful technique for visualizing and predicting phase assemblages and relative phase contents using three chemical compositions [35]. The oxide composition obtained via BSE for all samples was plotted as a CaO-Al_2O_3-SiO_2 ternary diagram. It is shown in Figure 11.

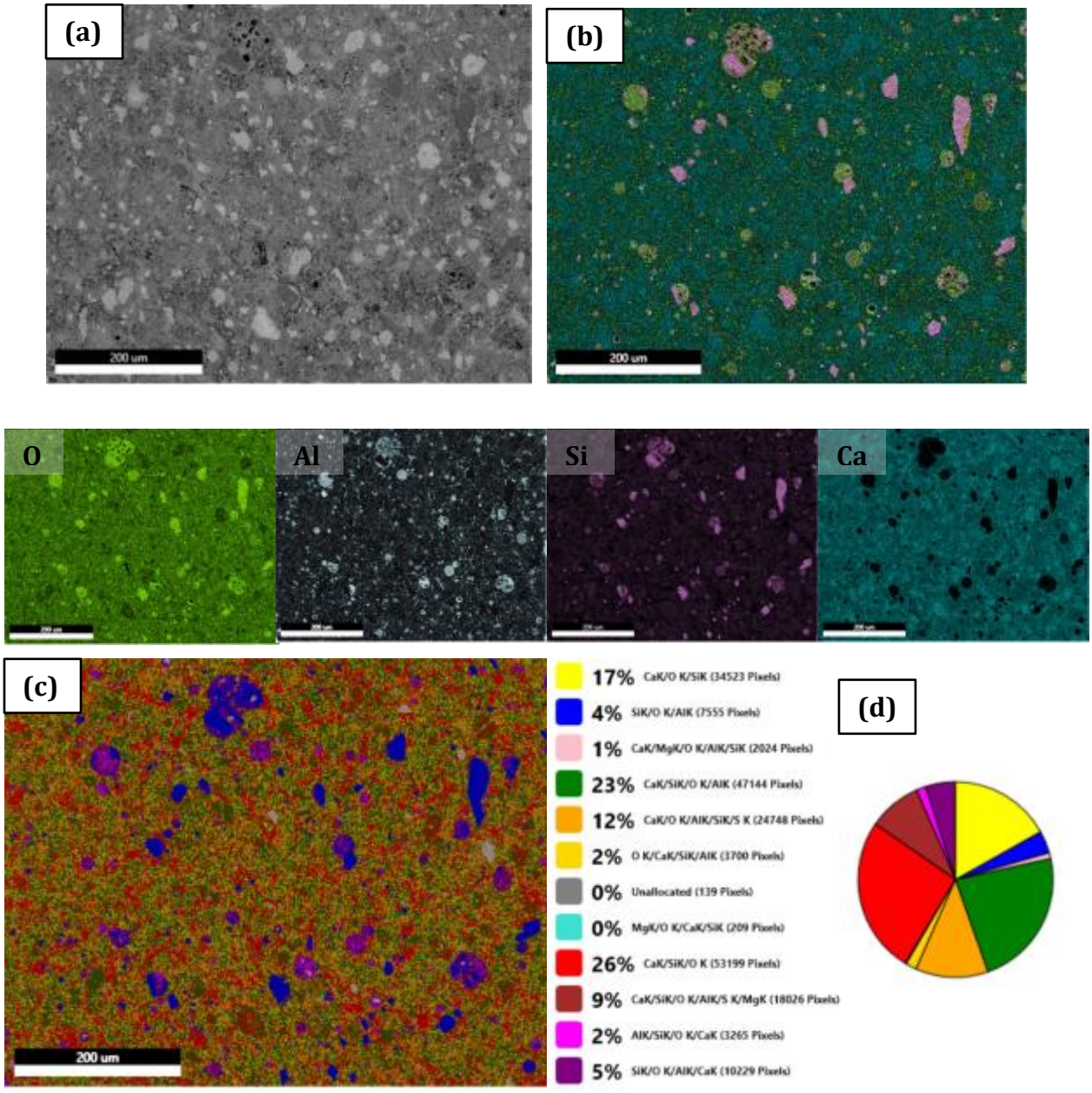

Figure 10. BSE analysis of the OPC+FA-LD sample after 28 days of curing, including (a) BSE image, (b) elemental composition mapping, (c) phase composition mapping using EDS analysis, and (d) pie chart depiction of phase composition

From the ternary phase diagram it can be noted that the addition of mineral additives (silica fume and fly ash) led to an increase in SiO_2 and a decrease in CaO_2. The OPC samples, therefore, can be classified as having high calcium content, with OPC+FA and OPC+SF having medium calcium contents. The data clearly indicates that the addition of SF increased the silica content, thereby increasing the formation of silicate in C-A-S-H gels, whereas the addition of fly ash formed C-A-S-H gel with higher alumina content. This suggests that the alumina content, in addition to the secondary C-S-H formed due to the addition of fly ash in Portland cements, helped to form the high-density phases that contributed to the higher relative strength among the OPC+FA samples.

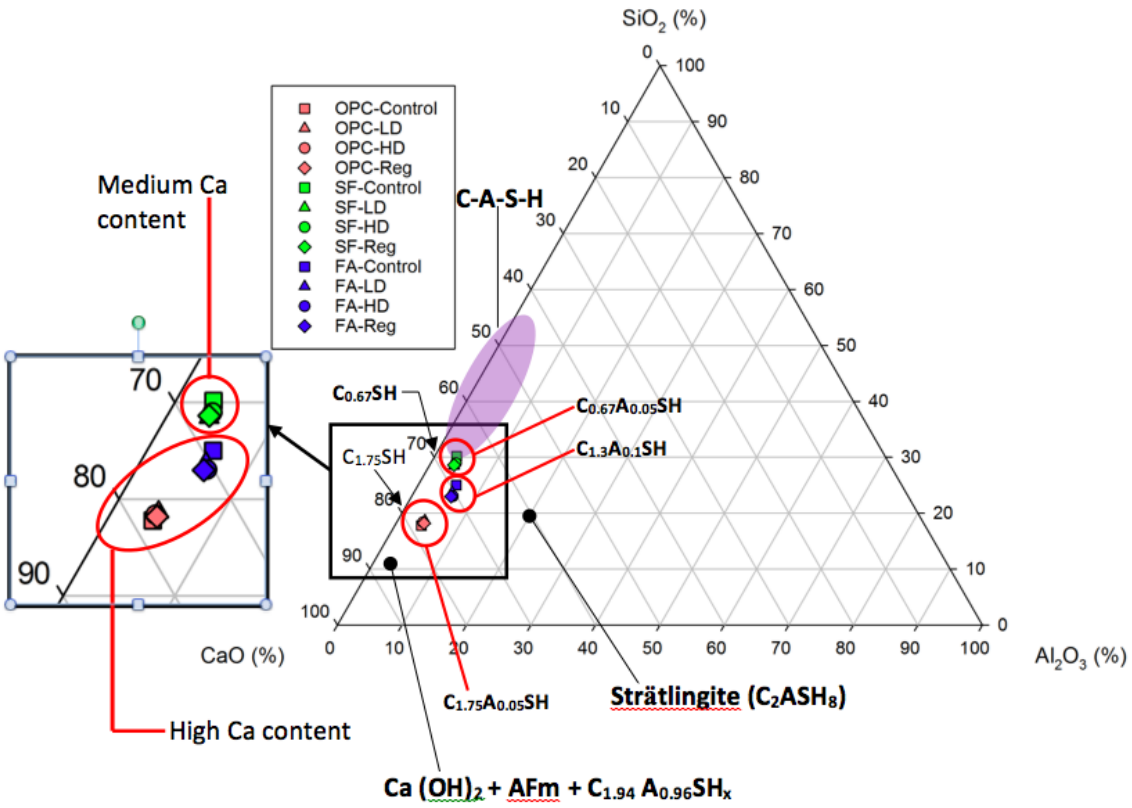

Figure 11. Bulk composition obtained via Energy Dispersive Spectroscopy (EDS) analysis plotted onto the $CaO–Al_2O_3–SiO_2$ ternary diagram. CaO is plotted in the left-side axis, Al_2O_3 on the bottom axis, and SiO_2 on the right-side axis.

4.4 X-Ray Microtomography (X-Ray µCT) Analysis

For the purpose of illustration, a volume of interest (VOI) was obtained from the original data set of each specimen, as shown for the OPC-LD sample in Figure 12. As an

example, the extracted volume is shown on a grey scale in Figure 12a, where black color shows the pores and white represents the densest phase. Because pore detection is difficult on the grey scale shown, the VOI image was then transformed, as shown in Figure 12b, in order to obtain the segmented porosity. This method involves separating the pore from the solid matrix by defining the range of grey scale—or, in this case, blue scale—that is associated with pore voxels. Here, segmented porosity refers to the extracted pore space after segmentation. Once segmented, pore connectivity can be revealed by determining whether or not adjacent pore voxels are in face-to-face contact and therefore connected to form a pore cluster. The percolating pore cluster is the the largest pore cluster that permeates in three orthogonal directions [36]. The percolating pore network relates to the effective porosity, as the interconnected part of the segmented porosity would most likely contribute to ingress of species such as chlorides and sulfates in the pores of the cement matrix. In other words, it is assumed that the largest percolating pore cluster represents the connected pores that most likely facilitate macroscopic transport within the cement matrix. The largest percolating pore cluster is assumed to be the connected pores that most likely contribute to the macroscopic transport in the cement matrix. This effective pore network is depicted in Figure 12c. Thus the panels within Figure 12 represent the intermediate stages of the porosity calculation.

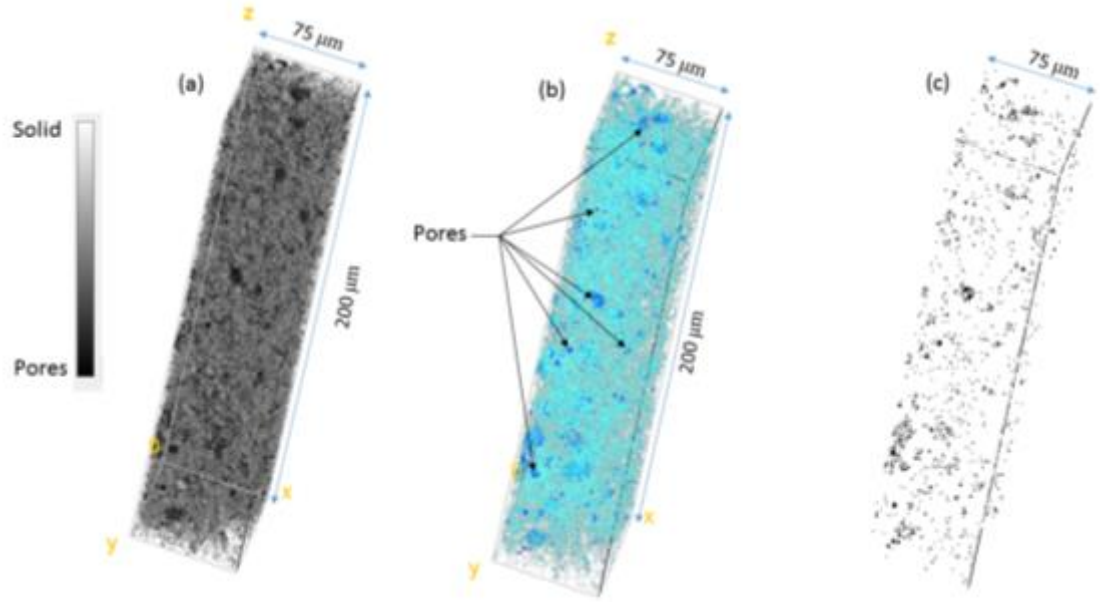

Figure 12. X-Ray microtomography analysis for the OPC+LD sample, including (a) extracted volume on a grey scale showing black as pores and white as solid, (b) detection of pores (blue color) in the sample that was used to obtain segmented porosity, and (c) effective pore network

The segmented porosities, obtained via a segmentation process using X-ray microtomography like the one described above, is shown in Figure 13. OPC-RP exhibited the highest porosity (0.38), whereas the OPC+FA-Ctrl sample showed the least

porosity (0.15). The results indicate that addition of fly ash and silica fume led to decreases in porosity as compared to OPC samples, which showed the highest porosity values. It should be noted that the addition of high dose irradiated plastic contributed to a decrease in segmented porosity for all three binder types when compared to the samples with regular plastic (OPC-RP, OPC+FA-RP, OPC+SF-RP). This suggests that the addition of irradiated plastic may have acted as a pore-blocking agent, in addition to its formation of chemical phases such as C-S-H and C-A-S-H, which contributed to the densification of the cementitious matrix.

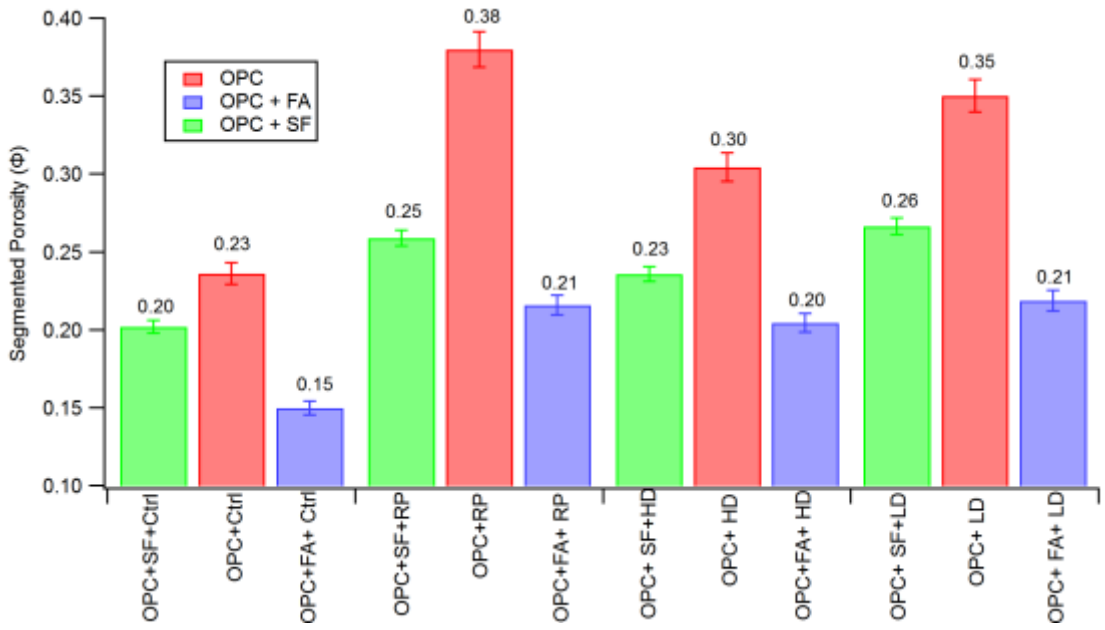

Figure 13. Segmented porosity obtained from X-ray microtomography data for all the samples. Samples containing FA or SF showed lower levels of porosity than did OPC samples. For all three cement binder types, the HD samples showed lower levels of porosity than did the RP samples.

4.5 Summary of Findings

Compression testing showed that a high dose irradiated plastic additive did indeed improve strength as compared to the effect of a regular, non-irradiated plastic. This suggests that irradiation is a viable potential solution for gaining back some of the strength that is lost when plastic is added to concrete. XRD analysis showed that various differences in C-S-H and C-A-S-H phase formation from the addition of both irradiated plastic and mineral additives helped to form the high-density phases that contributed to higher relative strength among the HD and LD samples. The discerning presence of the gismondine phase, in particular, suggests that the addition of irradiated plastic may have

caused a change in the structure of C-S-H gels and initiated the possible formation of unique C-A-S-H gels. This could explain, in part, the strength increases shown in the irradiated plastic-containing samples. BSE analysis showed that a higher alumina content among fly ash samples helped to form the high-density phases that contributed to higher relative strength among the fly ash samples, as evidenced in the ternary phase diagram. X-ray microtomography showed that the addition of high dose irradiated plastic consistently contributed to a decrease in segmented porosity, indicating that irradiated plastic may have acted as a pore-blocking agent. This effect is in addition to its formation of chemical phases such as C-S-H and C-A-S-H, which contributed to the densification of the cementitious matrix.

5 Conclusions

This study clearly showed the benefits of using gamma irradiated recycled plastic for strength gain in Portland cements. A thorough micro- and pore-structural analysis was performed in order to provide insight at an angstrom-level scale (through XRD) and at a micron-level scale (through BSE and microtomography). It was determined that incorporating high dose irradiated plastic into cement paste samples led to decreased porosity and increased compressive strength, which was attributed to the formation of C-A-S-H gels along with secondary C-S-H, which forms during the hydration processes.

By partially replacing Portland cement with a recycled waste material, this design, when scaled to the level of mass concrete production, could contribute to reduced carbon emissions and provide a long-term solution for waste plastic storage. Based on comparison with previous studies that used recycled plastic as an additive, it is clear that irradiation adds the benefit of increased compressive strength. Further research should be done to discover the true optimal combination of irradiated plastic and mineral additive for high strength. The groundwork, however, has been laid for the continued development of the ideas presented here.

5.1 Sources of Error and Future Work

One critical uncertainty within the experimentation process was the plastic particle size. The particles resulting from the extensive crushing process were far from uniform. The particles within the sample placed on the microscope slide for measurement ranged from being on the orders of 10 to 1,000. Additionally, using a mortar and pestle is in itself an inherently unreliable way of achieving a uniform particle size because it is difficult to control that the person crushing uses the same physical intensity for each batch of plastic. For these reasons, it is possible that the average particle sizes of the plastic that went into

each cement batch were very different. If particle size affects strength, these differences could have been a contributing variable to variation in strength.

Future studies should aim to improve the uniformity of the plastic size. This would allow for a clearer portrayal of how the irradiated plastic alone affects to strength, without the influence of other inconsistencies among samples. Furthermore, there are countless combinations of plastic dose and mineral additive that could be explored for the purpose discovering an optimal high strength combination, in addition to numerous variations in plastic type, plastic percent composition, plastic particle size, mineral additive percent composition, etc. It would also be of interest to test for variation in other mechanical properties, such as tensile strength, flexural toughness, impact resistance, and workability. These properties in particular have been shown in previous research be affected by the addition of plastic, so it would be useful to assess their responses to an irradiated plastic additive. Finally, a more thorough investigation of plastic recycling options—and specifically, whether or not this recycling alternative would truly be more energy efficient than mechanical recycling—is necessary in order to consider both the feasibly and the value of this idea in the context of mass concrete production.

6 Acknowledgements

Many individuals helped make this study possible. I would like to thank Dr. Kunal Kupwade Patil for his patience, guidance, expertise, resources, and willingness to help turn this idea into a real study. I would like to both credit and thank my partner in the 22.033 undergraduate design course, Michael Ortega, who developed this idea with me and contributed equally to the study through the compression-testing phase. I would also like to thank Professor Oral Büyüköztürk and the MIT Laboratory for Infrastructure Science and Sustainability (LISS) for their support of this work, as well as Professor Michael Short and Professor Anne White for their invaluable knowledge, mentorship, and encouragement throughout the process of developing this study. Many thanks also to Peter Brenton and the MIT Department of Nuclear Science and Engineering for their financial support, Mitch Galanek and MIT EHS for assistance with access to and use of the cobalt-60 facility, Stephen Rudolph for his help with compression testing, Charlie Settens for his many days of helping me understand XRD analysis, and Patrick Boisvert from the MIT SEM lab for assisting me with the BSE analysis. Finally, I would like to thank my grandfather, a concrete construction expert, for his inspiration and for passing down his interest to me.

Appendix A – Justification of Plastic Percent Composition

A constraint on the total number of samples that could be set and tested necessitated the selection of one ideal percent composition of plastic in the cement samples. Previous studies were reviewed in order to determine the composition at which plastic-enhanced concrete displays maximum strength. The findings are summarized in the Table 3. The given references can be found in the References section of this paper. Past research showed a general decrease in strength as the percent composition increased. No strength improvements were observed for plastic compositions beyond 1.5% by volume. For this study, a 1.25% composition by weight was chosen.

Table 3. Literature review for selection of percent plastic composition

Polymer added to cement	Percentage metric	Strength Type(s)	Trend	Reference Number
Not specified (general plastic)	Weight	Compressive, flexural, tensile	Steady decrease up to 20%	37
Polyethylene terephthalate	Volume	Compressive	Maximizes at 1%	38
Not specified (general plastic)	Weight	Compressive	Steady decrease up to 15%	39
Polyethylene terephthalate	Volume	Compressive, tensile	(Comp) steady decrease up to 50%, (tens) maximizes at 1.5%	40
Polycarbonate	Volume	Compressive, tensile	Steady decrease up to 50%	40

Appendix B – Justification of Dose Levels for Plastic Additive

Previous studies were reviewed in order to determine the dose levels for the irradiated plastic additive. Trends in strength with varying dose according to different studies are summarized in Table 4. The given references can be found in the References section of this paper. The irradiation type used in the study represented by the last row was electron-beam irradiation, while all others used gamma irradiation. The results for PET are somewhat inconsistent and suggest a need to test both high and low dose levels. A low dose and high dose of 10 kGy and 100 kGy, respectively, were selected for the testing in this study.

Table 4. Literature review for selection of high and low dose levels

Polymer	Strength Type	Trend	Maximum Strength Increase	Reference Number
Polyethylene	Tensile	Increase up to 10 kGy	Not specified	14
Polyethylene	Impact	Begins to fall at 70 kGy	Not specified	14
Polyethylene terephthalate	Tensile	Increases up to 150 kGy	Not specified	22
Polyethylene terephthalate	Compressive	Increases up to 100 kGy	35%	22
Polyethylene terephthalate	Mechanical	Increases up to 200 kGy	50%	22
Polyethylene terephthalate	Tensile	Increases up to 10 kGy	6%	23
Polyethylene terephthalate	Tensile	Maximizes at 60 and 105 kGy	19%	24

References

[1] Crow, James Mitchell. "The concrete conundrum." Chemistry World 5, no. 3 (2008): 62-66. Retrieved on 31 Oct. 2016. <http://www.rsc.org/images/Construction_tcm18-114530.pdf>.

[2] Worrell, Ernst, Lynn Price, Nathan Martin, Chris Hendriks, and Leticia Ozawa Meida. "Carbon dioxide emissions from the global cement industry 1." *Annual Review of Energy and the Environment* 26, no. 1 (2001): 303-329.

[3] Ali, M. B., R. Saidur, and M. S. Hossain. "A review on emission analysis in cement industries." *Renewable and Sustainable Energy Reviews* 15, no. 5 (2011): 2252-2261.

[4] Gu, Lei, and Togay Ozbakkaloglu. "Use of recycled plastics in concrete: A critical review." *Waste Management* 51 (2016): 19-42.

[5] EPA, 2014. Municipal Solid Waste Generation, Recycling, and Disposal in the United States Tables and Figures for 2012. Environmental Protection Agency, pp. 1-63. Retrieved on 11 May, 2017. < https://www.epa.gov/sites/production/files/2015-09/documents/2012_msw_dat_tbls.pdf>.

[6] Al-Salem, S. M., P. Lettieri, and J. Baeyens. "Recycling and recovery routes of plastic solid waste (PSW): A review." *Waste management* 29, no. 10 (2009): 2625-2643.

[7] Guilford, Gwynn. “A lot of US plastic isn’t actually being recycled since China put up its green fence.” Quartz, 16 Sept. 2013. Retrieved on 17 Dec. 2016. <qz.com/122003/plastic-recycling-china-green-fence/>.

[8] Yoshida, Aya. "China: The world’s largest recyclable waste importer." *World* 3, no. 4,000 (2005): 4-500.

[9] Corbett, James J., and Paul Fischbeck. "Emissions from ships." *Science* 278, no. 5339 (1997): 823-824.

[10] Choi, Yun-Wang, Dae-Joong Moon, Jee-Seung Chung, and Sun-Kyu Cho. "Effects of waste PET bottles aggregate on the properties of concrete." *Cement and Concrete Research* 35, no. 4 (2005): 776-781.

[11] Pelisser, Fernando, Oscar Rubem Klegues Montedo, Philippe Jean Paul Gleize, and Humberto Ramos Roman. "Mechanical properties of recycled PET fibers in concrete." *Materials research* 15, no. 4 (2012): 679-686.

[12] Saikia, Nabajyoti, and Jorge de Brito. "Waste polyethylene terephthalate as an aggregate in concrete." *Materials Research* 16, no. 2 (2013): 341-350.

[13] Jog, J. P. "Crystallization of polyethyleneterephthalate." *Journal of Macromolecular Science, Part C: Polymer Reviews* 35, no. 3 (1995): 531-553.

[14] Plester, David W. "The Effects of Radiation Sterilization on Plastics." P2 InfoHouse. Plastics Division, Imperial Chemical Industries, n.d. Retrieved on 31 Oct. 2016. <http://infohouse.p2ric.org/ref/27/26567.pdf>.

[15] Kattan, Munzer. "Thermal behavior of gamma- irradiated amorphous poly (ethylene terephthalate) films." *Polymer Engineering & Science* 46, no. 10 (2006): 1374-1377.

[16] Demirel, Bilal, Ali Yaraş, and Hüseyin Elçiçek. "Crystallization behavior of PET materials." *Balıkesir Üniversitesi Fen Bilimleri Enstitüsü Dergisi* 13, no. 1 (2016): 26-35.

[17] Muhit, I. B., S. S. Ahmed, M. M. Amin, and M. T. Raihan. "Effects of Silica fume and Fly ash as partial replacement of cement on water permeability and strength of high performance concrete." In *4th International Conference on Advances in Civil Engineering, AETACE, Association of Civil and Environmental Engineers*. 2013.

[18] Roy, D. M., P. Arjunan, and M. R. Silsbee. "Effect of silica fume, metakaolin, and low-calcium fly ash on chemical resistance of concrete." *Cement and Concrete Research* 31, no. 12 (2001): 1809-1813.

[19] Duval, R., and E. H. Kadri. "Influence of silica fume on the workability and the compressive strength of high-performance concretes." *Cement and concrete Research* 28, no. 4 (1998): 533-547.

[20] Wankhede, P. R., and V. A. Fulari. "Effect of fly ash on properties of concrete." *International Journal of Emerging Technology and Advanced Engineering (IJETAE), ISSN* (2014): 2250-2459.

[21] ASTM, 2004. ASTM C 618 Standard Specification for Coal Fly Ash and Raw or Calcined Natural Pozzolan for Use as a Mineral Admixture in Concrete. Annual Book of ASTM Standard, Section 4.

[22] Martínez-Barrera, Gonzalo, Liliana Ivette Ávila-Córdoba, Miguel Martínez-López, Eduardo Sadot Herrera-Sosa, Enrique Vigueras-Santiago, Carlos Eduardo Barrera-Díaz, Fernando Ureña-Nuñez, and Nelly González-Rivas. "Gamma Radiation as a Recycling Tool for Waste Materials Used in Concrete." *Evolution of Ionizing Radiation Research, ISBN* (2015): 978-953-51-2167-1.

[23] Jeon, Dae Hoon, Kwang Ho Lee, and Hyun Jin Park. "The effects of irradiation on

physicochemical characteristics of PET packaging film." *Radiation Physics and Chemistry* 71, no. 5 (2004): 1059-1064.

[24] Oliveira, Vitor M., Angel V. Ortiz, Nélida L. Del Mastro, and Esperidiana AB Moura. "The influence of electron-beam irradiation on some mechanical properties of commercial multilayer flexible packaging materials." *Radiation Physics and Chemistry* 78, no. 7 (2009): 553-555.

[25] Ávila Córdoba, Liliana, Gonzalo Martínez-Barrera, Carlos Barrera Díaz, Fernando Ureña Nuñez, and Alejandro Loza Yañez. "Effects on mechanical properties of recycled PET in cement-based composites." *International Journal of Polymer Science* 2013 (2013).

[26] Varlashkin, P. "Approaches to quantification of amorphous content in crystalline drug substance by powder X-ray diffraction." *American Pharmaceutical Review* 14, no. 1 (2011).

[27] Zemajtis, Jerzy Z. "Role of Concrete Curing." *Portland Cement Association, Skokie* (2014). Retrieved on 18 Nov. 2016. <http://www.cement.org/for-concrete-books-learning/concrete-technology/concrete-construction/curing-in-construction>.

[28] ASTM, 2016. ASTM C-39, Standard Test Method for Compressive Strength of Cylindrical Concrete Specimens. ASTM International.

[29] Jagodzinski, H. "HP Klug und LE Alexander: X- ray Diffraction Procedures for Polycrystalline and Amorphous Materials, 2. Auflage. John Wiley & Sons, New York- Sydney- Toronto 1974, 966 Seiten, Preis:£ 18.55." *Berichte der Bunsengesellschaft für physikalische Chemie* 79, no. 6 (1975): 553-553.

[30] Guthrie, George D., and J. William Carey. "A thermodynamic and kinetic model for paste–aggregate interactions and the alkali–silica reaction." *Cement and Concrete Research* 76 (2015): 107-120.

[31] De Silva, P. S., and Fredrick P. Glasser. "Phase relations in the system CaO- Al2O3- SiO2- H2O relevant to metakaolin-calcium hydroxide hydration." *Cement and concrete research* 23, no. 3 (1993): 627-639.

[32] Biagioni, Cristian, Elena Bonaccorsi, Stefano Merlino, and Danilo Bersani. "New data on the thermal behavior of 14Å tobermorite." *Cement and Concrete Research* 49 (2013): 48-54.

[33] Scrivener, Karen, Ruben Snellings, and Barbara Lothenbach, eds. *A Practical Guide to Microstructural Analysis of Cementitious Materials*. Crc Press, 2015. Retrieved on 17 May, 2017. < http://www.crcnetbase.com/doi/pdf/10.1201/b19074-1>.

[34] Scrivener, Karen L. "Backscattered electron imaging of cementitious microstructures: understanding and quantification." *Cement and Concrete Composites* 26, no. 8 (2004): 935-945.

[35] HERFORT, DUNCAN, and BARBARA LOTHENBACH. "Ternary phase diagrams applied to hydrated cement." In *A Practical Guide to Microstructural Analysis of Cementitious Materials*, pp. 485-502. CRC Press, 2015.

[36] Promentilla, Michael Angelo B., T. Sugiyama, T. Hitomi, and N. Takeda. "Quantification of tortuosity in hardened cement pastes using synchrotron-based X-ray computed microtomography." *Cement and Concrete Research* 39, no. 6 (2009): 548-557.

[37] Batayneh, Malek, Iqbal Marie, and Ibrahim Asi. "Use of selected waste materials in concrete mixes." *Waste management* 27, no. 12 (2007): 1870-1876.

[38] Nibudey, R. N., P. B. Nagarnaik, D. K. Parbat, and A. M. Pande. "A model for compressive strength of PET fiber reinforced concrete." *American Journal of Engineering Research* 2, no. 12 (2013): 367-372. *e-ISSN : 2320-0847.*

[39] Rai, Baboo, S. Tabin Rushad, Bhavesh Kr, and S. K. Duggal. "Study of waste plastic mix concrete with plasticizer." *ISRN Civil Engineering* 2012 (2012).

[40] Hannawi, Kinda, Siham Kamali-Bernard, and William Prince. "Physical and mechanical properties of mortars containing PET and PC waste aggregates." *Waste management* 30, no. 11 (2010): 2312-2320.